Desalination and Water Treatment
www.deswater.com

doi: 10.5004/dwt.2017.21264

85 (2017) 282–290
August

Visible light driven photocatalysis for water purification by highly crystalline multiferroic $BiFeO_3$ nanoparticles synthesized via wet chemical route

Sajjad Ahmad[a], Fizza Naseem[a], Muhammad Shahid[a], Imran Shakir[b], Mohamed F.A. Aboud[b], Mansoor Sarfraz[b], Muhammad Azhar Khan[c], Aziz Ur Rehman[a], Muhammad Farooq Warsi[a,*]

[a]*Department of Chemistry, The Islamia University of Bahawalpur, Bahawalpur 63100, Pakistan, Tel. +92 300 6342261; Fax: +92 62 9255474; emails: farooq.warsi@iub.edu.pk (M.F. Warsi), chsajjadahmad@hotmail.com (S. Ahmad), fizza915@gmail.com (F. Naseem), shahid@iub.edu.pk (M. Shahid), azizypk@yahoo.com, (A.U. Rehman)*
[b]*Sustainable Energy Technologies Center, College of Engineering, King Saud University, Riyadh, Saudi Arabia, emails: imranskku@gmail.com (I. Shakir), maboud@ksu.edu.sa (M.F.A. Aboud), smansoor@ksu.edu.sa (M. Sarfraz)*
[c]*Department of Physics, The Islamia University of Bahawalpur, Bahawalpur 63100, Pakistan, email: azhar.khan@iub.edu.pk*

Received 19 January 2017; Accepted 23 July 2017

ABSTRACT

$BiFeO_3$ (BFO) multiferroics were synthesized via a low-cost wet chemical method. The enigma involved the optimization of different reaction conditions. A comprehensive study was carried out to optimize the reaction conditions such as molar ratios of surfactant with total concentration of precursors, chemical source and solubility of precursors and annealing temperature. A pragmatic nucleation of precursors was achieved at molar proportions 1:1 between cetyltrimethylammonium bromide (CTAB) and total molar concentration of precursors. An endeavor approach was made to accomplish the appropriate flexibility of emulsion phase by adding small quantity of ethanol as a co-surfactant, nevertheless the solubility of $Bi(NO_3)_3$/$BiCl_3$ was unfavorably affected. Subsequently, the single phase product of BFO was observed with reaction conditions 1:1 molar concentration ratio between precursors and CTAB, with precursors $BiCl_3$ and $Fe(NO_3).9H_2O$ and annealing temperature of 900°C for a time of 7 h. The structural elucidation was made by comparing the extracted data with standard cards (ICDD - 01-086-1518) of XRD. The crystallite size was computed to be 18 nm. The DC conductivity was found to be 1.005×10^{-9} S cm^{-1}. The optical band gap was found in the range of ~2.6 eV. Keeping in view the optical band gap, BFO nanoparticles were investigated for photocatalytic degradation of Congo Red dye under visible light. The photocatalytic degraded sample was investigated through the high-performance liquid chromatography (HPLC) and chemical oxygen demand estimation (COD value) for treated sample was calculated to be 63.27% which is less than the untreated sample which disclosed a photodegradation of Congo Red dye into simple hydrocarbon products as perceived in HPLC–chromatogram. The post XRD data showed the stability of BFO which could be separated through a simple bar magnet from reaction container.

Keywords: Visible light; Photocatalysis; Nanoparticles; Micro-emulsion

1. Introduction

The multiferroics materials have unique characteristics of combining both electrical and magnetic properties simultaneously in the same material and manipulating in a way that one can control another [1,2]. BFO is a prominent multiferroic which simultaneously possesses ferroelectric, ferromagnetic and anti-ferromagnetic (G-type) order at and above room temperature. BFO has been considered as a standard material in the global research for new multiferroic materials. However, the practical use of BFO in fabrication

* Corresponding author.

1944-3994/1944-3986 © 2017 Desalination Publications. All rights reserved.

of real devices is limited up till now due to some problems associated with fabrication of single phase BFO. The high leakage current density, spiral anti-ferromagnetic spin arrangements and low remittance magnetic density are needed to be resolved [3,4]. One helpful way to overcome these problems is to prepare the pure phase BFO. The inclusion of impurities during the synthesis of BFO could be controlled by adopting suitable synthetic strategy. Several synthesis routes of BFO have been reported in the literature (solid state and wet chemical techniques). Initially, the synthesis of metal oxides was carried out with solid-state method which was based on direct reaction of solid-state homogenized powder mixture of reactants. A high temperature was applied during synthesis and the reaction product was completely controlled by the mobility of ionic or atomic species within the reactants and the product [5]. In solid-state method, high temperature and small particle size of reactants are required for maximum mobility of reacting species with reaction mixture and only thermodynamically stable phases are existed. Solid-state reaction scheme is a pioneer method in fabrication of BFO materials but impurities are also reported in the final products [6]. In contrast to ceramic approach, the wet chemical synthesis provides surprising control of size and homogeneity of nanoparticles. The wet chemical method is further divided into different modes depending on reaction pathway. There are different wet chemical methods reported in the literature such as sol-gel, co-precipitation, hydrothermal synthesis, microwave hydrothermal synthesis, sono-chemical and micro-emulsion synthesis. The most common wet chemical method is sol-gel method, in which the mobility of metal ions is reduced by sol-gel reaction medium [7]. The sol-gel method is commonly used in the synthesis of bulk metal oxides such as ceramics, glasses, films and fibers [8].

In wet chemical methods, the micro-emulsion method is also an emerging route in nanomaterials synthesis. Schulman et al. [9] prepared a quaternary solution of water, benzene, hexanol and potassium oleate which was stable and homogenous but slightly opaque. This solution was purposed as micro-emulsion. Micro-emulsions are categorized as colloidal solutions in which nanodispersions of oil in water or water in oil stabilized by surfactant which form an interfacial film separating the polar and the non-polar domains [9], play vital role in controlling the nanostructures. The nanoemulsions have the droplet size in the range of 20–200 nm and have a unique characteristic to behave like a nanoreactor [10,11]. It has been observed that micro-emulsions are isotropic, homogeneous and thermodynamically stable solutions. In an aqueous micro-emulsion (oil in water [o/w]), the hydrophobic domain forms small droplets with almost homogenized size and morphology which act as nanoreactors [12]. CTAB is a well-known surfactant which is used in micro-emulsion systems with different reagents and co-surfactants for the synthesis of nanomaterials. In 1999, Fangand Yang synthesized ZrO_2-Y_2O_3 nanoparticles by using CTAB/hexanol/water micro-emulsion [13].

Due to the dynamic nature of micro-emulsion, the droplets are in Brownian motion, collisions occur among the droplets which results in fused dimmers and interchange reactants within a dimmer at a rate constant K_{ex}. The exchange of reactants within dimmer could be controlled by flexibility of surfactant. The exchange of precursor ions is limited and takes place at interface of both the domains stabilized by the surfactants. Consequently, a product with narrow size distribution is obtained [14–16].

A dramatic change has been observed in the properties of nanomaterials as compared with their bulk analogues for various applications including solar energy harvesting. Researchers are continuously working to explore the efficient and low-cost photosensitive materials for utilizing the marvellous source of energy in nature, that is, the Sun. Therefore, the materials which have the optical band gap in the range of <3 eV are suitable for sunlight trapping [17]. No doubt, silicon diodes are the renowned photovoltaic active materials and are being employed from last several decades as solar energy harvesters [18]. The materials without the body centered crystal structures are associated with ferroelectricity and showed optical band gap in the UV/Visible region [19]. However, in last few years, some efficient materials had been developed for photocatalysis which possessed not only photocatalytic potential but also magnetic properties which could be used for the recovery of photocatalytic material [20].

It has been observed that perovskite materials showed a significant efficiency for photoharvesting. The mechanism involved the absorption of light with characteristic wavelength. The absorption of light would enhance the excitation of electrons followed by increased transient photocurrent. It was accentuated to synthesize photocatalyst with significant working efficiency and naturally sustainable with sunlight to quash the common organic pollutants of industrial wastewater. BFO nanoparticles showed optical energy band gap of ~2.6 eV which is associated with photoenergy of visible region. Photocatalysis involves the absorption of a particular band of light and production of electron–hole pairs on the surface of photocatalyst material which eventually accelerate the production of free radicals in the reaction mixture. The reactive species (free radicals) oxidized the organic compounds. In photocatalytic phenomena, the activity is significantly dependent on surface area, optical band gap of material and rate of electron–hole pair recombination [21].

2. Experimental setup

The main focus of research study was to develop an innovative, low cost but efficient pathway for the synthesis of pure phase BFO by wet chemical method, "microemulsion." In present research work, CTAB was selected as an emulsifier and allied reaction conditions were optimized for significant parameters which could influence the pure phase of BFO. The following chemicals were used as a precursor sources without any further purification: $Fe(NO_3)_3.9H_2O$ (Sigma-Aldrich, Europe/Germany, 98%), $Bi(NO_3)_3.5H_2O$/ $BiCl_3$ (Sigma-Aldrich, 99%), CTAB (Amresco, Canada, 98%) and aqueous NH_3 (BDH 35%) (Sigma-Aldrich, 98%). All the reagents were prepared in deionized water with successive decrease or increase in CTAB and reagent concentrations. 100 mL solution of each reagent was measured in separate beaker. These were stirred and heated up to 60°C. After attaining the set temperature, 100 mL solution of CTAB was added into the ferric nitrate solution and stirred for few minutes. The total volume of reaction mixture was 300 mL

and it was constant in the whole study. Then an acidic solution of $BiCl_3$ with pH 1.3 was added in the reaction mixture. Immediately a light yellow dense suspension of CTAB was developed in reaction mixture. Aqueous ammonia (2 M) solution was dropped with burette and pH of reaction mixture continuously monitored up to 10.5. The addition of ammonia solution was stopped and the whole reaction mixture was stirred for further 5 h. The reaction mixture was allowed to settle down for 12 h. The precipitates were washed with deionized water several times till the pH of the medium becomes neutral. Then the drying was carried out at a temperature of 100°C. The dried product precipitates were grinded by agate mortar and pestle. Then each trial batch was divided into three fractions for annealing at three different temperatures.

The effects of various parameters on synthesis of single phase BFO were systematically studied and optimized. The significant parameters such as concentration of surfactant CTAB, addition of co-surfactant (ethanol), composition of bismuth precursor and their solubility in water, annealing temperature and time of stirring were optimized. The synthesis of nanoparticles is illustrated in Fig. 1.

The whole study was allocated into four batches with same general synthesis procedure but a successive increase or decrease was made in optimizing parameters. A small quantity of synthesized sample BFO-(i) was subjected to TGA (thermogravimetric analysis). For each trial batch, the annealing temperature was kept in the range of 800°C–900°C. Different batches under certain conditions were synthesized as explained in each batch.

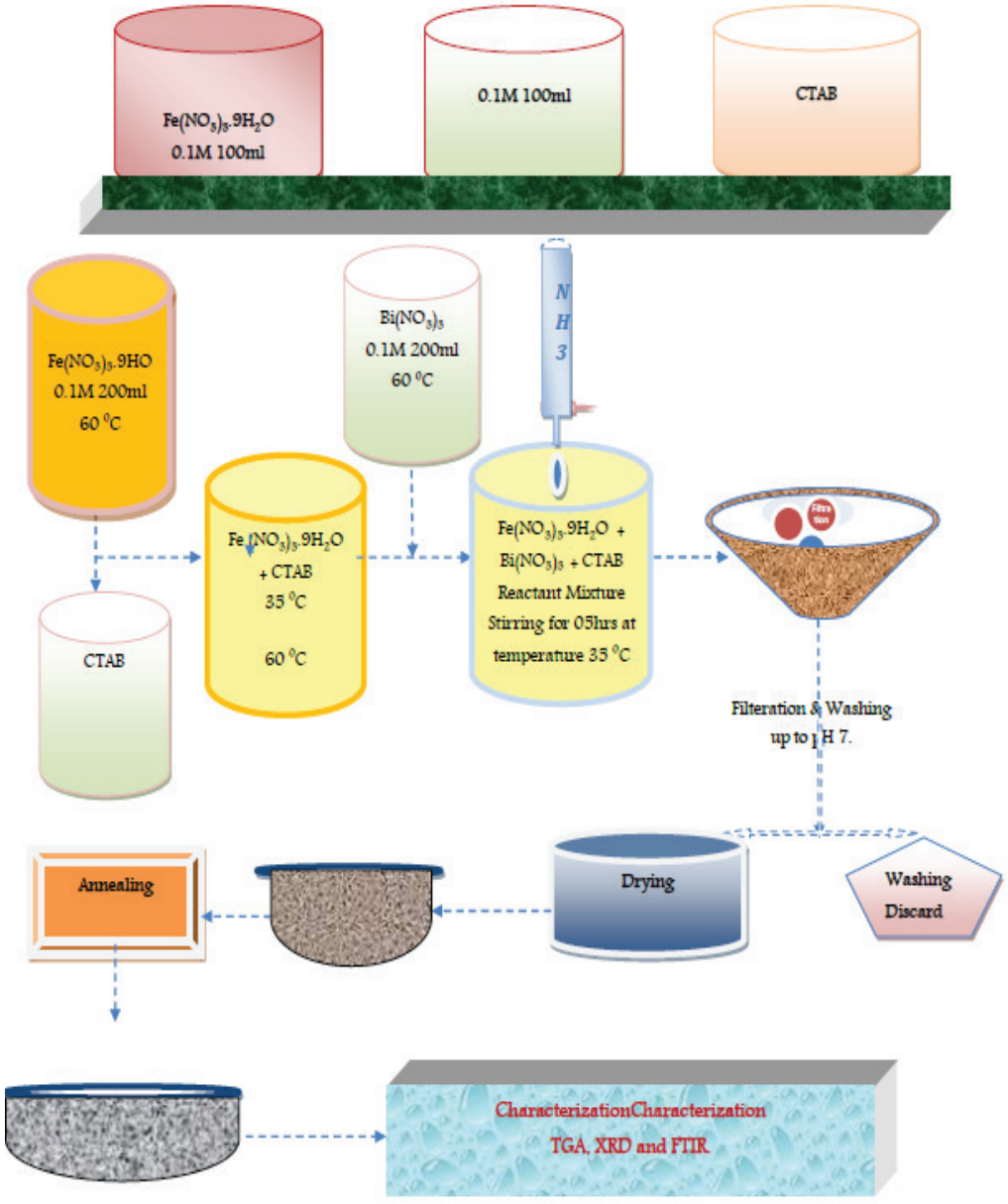

Fig. 1. Schematic diagram of wet chemical method of BFO synthesis by using single surfactant CTAB.

2.1. BFO batch-(i)

BFO was synthesized by adopting the aforementioned standard procedure using following chemicals: $Fe(NO_3)_3.9H_2O$ (Sigma-Aldrich, 98%), $Bi(NO_3)_3.5H_2O$ (Sigma-Aldrich, 99%), CTAB (98%, Amresco) and aqueous NH_3 (BDH 35%) (Sigma-Aldrich, 98%). The molar ratios of precursors and surfactant were kept as 1:1.5, respectively. It was observed that at molar ratios 1:1.5, a dense suspension was developed and the proper stirring was not achieved. The trial batch sample was divided into three parts and each part was annealed at 800°C, 850°C and 900°C separately for 7 h.

2.2. BFO batch-(ii)

In this batch, an attempt was made to increase the flexibility of surfactant for proper stirring. All the reagents and surfactants are same but only a small quantity of co-surfactant (lower number alcohol), ethanol, was added (20 cm^3 in total volume of 300 cm^3) to increase the flexibility of surfactant. All other steps were repeated according to general synthesis scheme. Physically, a fair stirring was observed and a dark brown product was obtained. The product was subjected to sintering and characterized by XRD.

2.3. BFO batch-(iii)

In this batch, the reaction parameters were slightly changed. The concentration of surfactant was adjusted as equal molar ratio to the total concentration of precursors and $BiCl_3$ was used as source of bismuth. The same annealing conditions were applied for each fraction.

2.4. BFO batch-(iv)

The 4th batch was synthesized by adopting the described standard procedure scheme but only the composition of bismuth source was replaced with $Bi(NO_3)_3.5H_2O$ (Sigma-Aldrich, 99%) instead of bismuth chloride. Following chemicals were used as received for this batch: $Fe(NO_3)_3.9H_2O$ (Sigma-Aldrich, 98%), $Bi(NO_3)_3.5H_2O$ (Sigma-Aldrich, 99%,), CTAB (98%, Amresco) and aqueous NH_3 (BDH 35%) (Sigma-Aldrich, 98%). The molar concentration of surfactant and precursors was kept similar to 3rd batch.

3. Results and discussion

All the as-prepared four batches of BFO were characterized by thermogravimetric analysis (TGA), Fourier-transformed infrared spectroscopy (FTIR) and powder X-ray diffraction (XRD) for structural elucidation.

3.1. Thermogravimetric analysis

The TGA and DSC (differential scanning calorimetric) thermograms were recorded on a simultaneous TGA/DSC instrument model "SDT Q600 V8.2 Build 100 thermal analyzer" at a heating rate of 10°C/min from 30°C to 850°C. The thermogram showed an initial weight loss of 8% at 73°C due to loss of water contents. A sharp change in thermogram was observed in the temperature range 110°C–330°C which was due to loss of water contents and decomposition of precursor nitrates. Similarly an exothermic peak was observed in DSC thermogram at 445°C which might be due to metal oxides reaction. The percentage weight loss of 10% was observed in the temperature range 445°C–740°C and there was no further weight loss upon heating. The total weight loss during thermal analysis between the temperature range 40°C–900°C was ~26% which occurred through different phases in the formation of perovskite structure [22]. The main purpose of TGA is to probe the annealing temperature that was found to be 900°C for BFO. The annealing of the samples was carried out in a controlled muffle furnace Vulcan A-550 at the temperatures 800°C, 850°C and 900°C. The thermograms are shown in Fig. 2(a).

3.2. FTIR analysis

The optimized sample BFO-(iv)-03 was subjected to spectral characterization. The FTIR spectroscopic analysis of synthesized sample was performed within the frequency range of 4,000–400 cm^{-1} at room temperature. The characteristic spectral bands of metal oxygen observed in the range ~400–600 cm^{-1} confirmed the formation of BFO nanoparticles [23]. Fe–O stretching vibrations in FeO_6 octahedral unit occur at wave number ~550 cm^{-1}. Fe–O and Bi–O bending vibrations occur at ~441 and ~449 cm^{-1}, respectively. A wide spectral in the range ~420–450 cm^{-1} was found which is attributed to the bending vibrations of both Fe–O and Bi–O present in FeO_6 and BiO_6 octahedral units, respectively. These spectral bands are shown in Fig. 2(b).

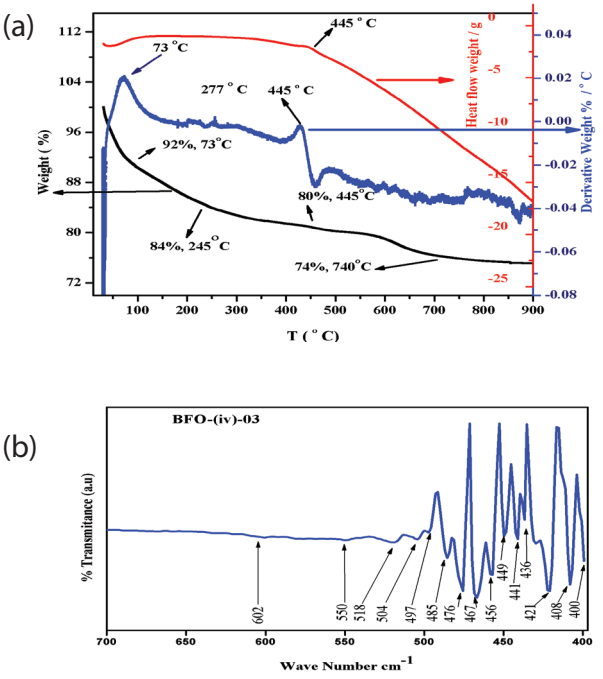

Fig. 2. (a) TGA, differential thermal analysis and DSC thermograms of optimized sample BFO-(iv)-03. (b) FTIR spectrum of optimized sample BFO-(iv)-03.

3.3. Structural analysis

The structural elucidation of all the synthesized batches was performed with the help of XRD technique and these patterns are shown in Fig. 3. The recorded XRD patterns of 1st batch, BFO-(i), were compared with standard card. It was found that all three XRD patterns showed main peaks at 2θ = 35°. Few traces of secondary phase were also observed (Bi_2O_3, Fe_2O_3 and $Bi_2Fe_4O_9$). The XRD patterns of BFO (annealed at three different temperatures) indicated the occurrence of impurity phases. However, remarkable peaks (peaks bearing high intensity) were observed with increase in temperature from 800°C to 900°C.

The XRD patterns of 2nd batch BFO-(ii)-03 revealed improved results as compared with 1st batch (all three samples). However, the main peak was observed at 39° which exhibited deviation with the standard BFO XRD pattern.

The 3rd batch, BFO-(iii), was synthesized by keeping in view the aforementioned results of the XRD patterns. Following steps were taken as follows: the concentration of CTAB was changed and this time it was used equal molar ratios (1:1) between the CTAB and total molar concentration of precursors. Physically an appropriate stirring was observed at 35°C without co-surfactant. Same procedure was repeated for annealing and XRD characterization. The characteristic diffraction patterns of BFO were observed at 2θ values ~22°, 31° and 32°. Although a prominent secondary phase peaks at 29° and 35° were also recorded in the samples. It was also noted that all three samples of 3rd batch show sharp peaks which were not evidenced in 1st and 2nd batches.

In 4th batch, all the reaction conditions remained persistent as followed in 3rd batch (CTAB concentration and volume 0.2 M/100 mL, precursor concentration 0.1 M/100 mL each, ammonia solution 2 M and annealing temperature ranges from 800°C to 900°C. The source of bismuth (Bi) was altered in this batch. In this batch, $BiCl_3$ was used instead of $Bi(NO_3)_3.5H_2O$. The XRD patterns of this batch displayed more sharp peaks which are comparable with the standard pattern of BFO. In this batch, few of the impurity phase peaks were also obsoleted in the samples which were annealed at 800°C and 850°C, respectively. However, more sharp peaks were noticed for BFO-(iv)-03 sample in which ignorable impurities were observed. The XRD pattern of BFO-(iv)-03 was matched with standard data card (ICDDO -01-086-1518) of BFO. The structural and physical parameters were calculated using XRD data (BFO-(iv)-03) and all these parameters are tabulated in Table 1.

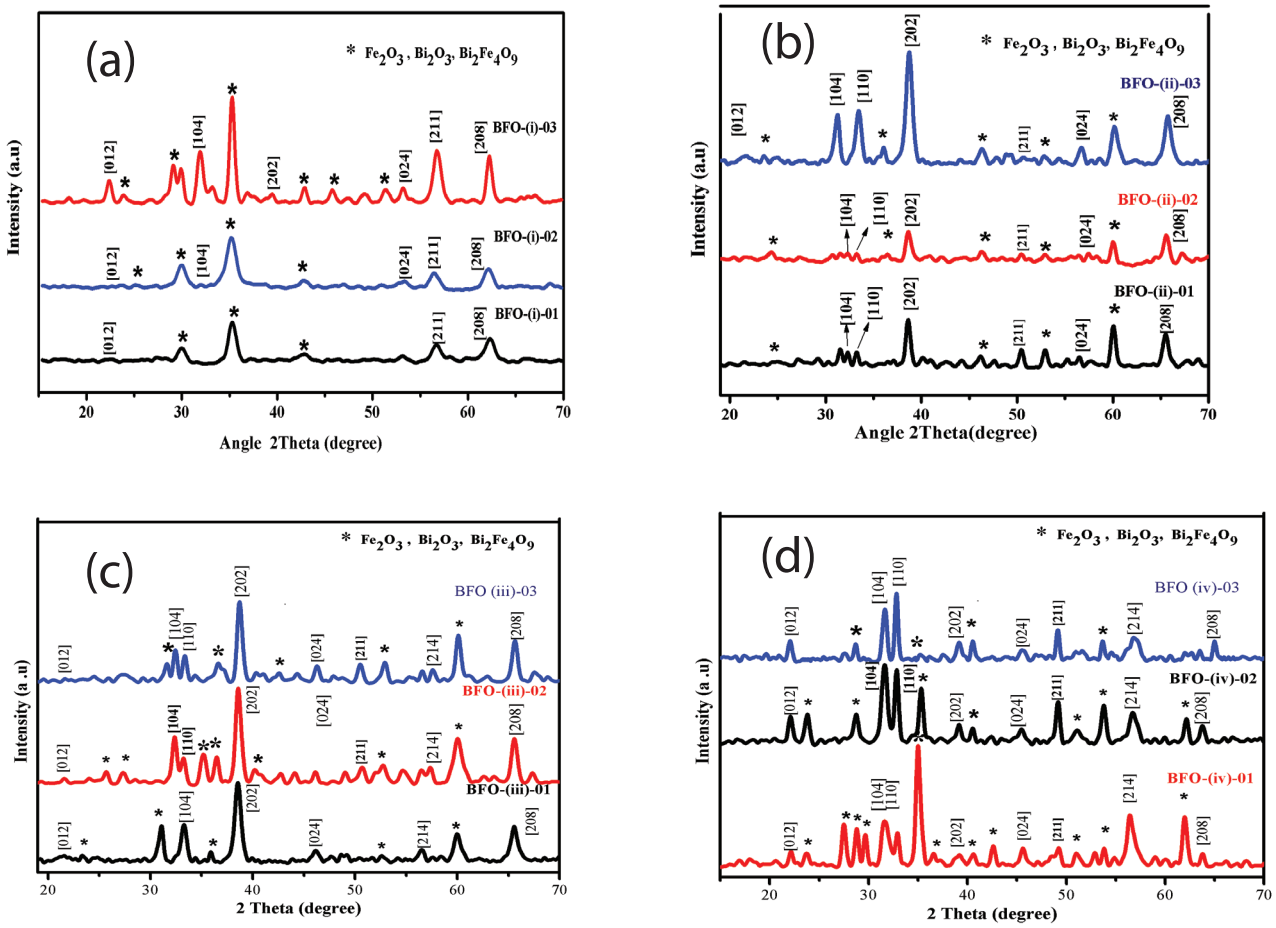

Fig. 3. XRD spectra for different batches, each batch is further divided into 1, 2 and 3 samples and annealed at temperatures 800°C, 850°C and 900°C, respectively. (a) BFO batch-(i), (b) BFO batch-(ii), (c) BFO batch-(iii) and (d) BFO batch-(iv).

3.4. Current–voltage analysis

Pure phase BFO ceramics show the semiconductor behavior. The insulating behavior decreases with the presence of impurities. It was reported that high conductivity of BFO is due to movement of oxygen vacancies. During the synthesis process, oxygen vacancies are produced by variation of Fe^{+3} to Fe^{+2} states [24]. The electrical resistivity was measured by I-V measurements by applying Eq. (1):

$$\rho = [R\ (\pi r^2)/l]\ \Omega\ \text{cm} \quad (1)$$

Similarly the conductivity of the sample was measured by Eq. (2):

$$\sigma = [1/\rho]\ \text{S cm}^{-1} \quad (2)$$

The conductivity of optimized sample BFO-iv-03 was found to be 10.506×10^{-10} S cm^{-1}. The current–voltage (I-V) plot is shown in Fig. 4.

4. Photocatalytic activity of BFO nanoparticles

After structure elucidation, the optimized product (BFO-(iv)-03) was applied for photocatalytic activity. The photocatalytic activity of optimized sample (BFO-(iv)-03) nanoparticles was studied by setting an experiment of photocatalytic degradation of Congo Red. The Congo Red dye was used as model organic compound because it is readily available and exhibits well-resolved visible spectrum. The mechanism involves the excitation of valance electrons to the conduction band by absorbing the sunlight of the photocatalyst material. Ultimately electron–hole pairs are generated on the surface of BFO nanoparticles. Most of the photocatalytic reactions are carried out in the aqueous medium and active species of OH• (radicals) are produced which are the good oxidants. Then in second step these are converted into specie of •OOH by attacking on holes [25].

$$BiFeO_3 + h\upsilon \rightarrow (\text{electron}^-_{CB} + \text{holes}^+_{VB})$$
$$(\text{electron}^-_{CB} + \text{holes}^+_{VB}) + \text{Congo Red} \rightarrow \text{degraded product}$$

The mechanism of photocatalytic process is illustrated in Fig. 5.

The fabricated ceramic was scanned for UV/Visible spectrum by using Agilent Cary-60 spectrophotometer. A well-defined absorption peak was observed in near visible region as shown in Fig. 6(a). From UV/Visible spectrum, the optical band gap was calculated (~2.6 eV) by applying the Tauc plot [26] as shown in Fig. 6(b).

Table 1
Table for lattice characteristic parameters of BFO-(iv)-03

Sample ID	BFO-IV-03
Lattice constants	
a (Å)	5.5529
b (Å)	5.5529
c (Å)	14.1280
X-ray density	9.72
Cell volume (Å^3)	435.6387
Bulk density (g cm^{-3})	3.0245
Porosity	0.643
Crystallite size (nm)	18.3546

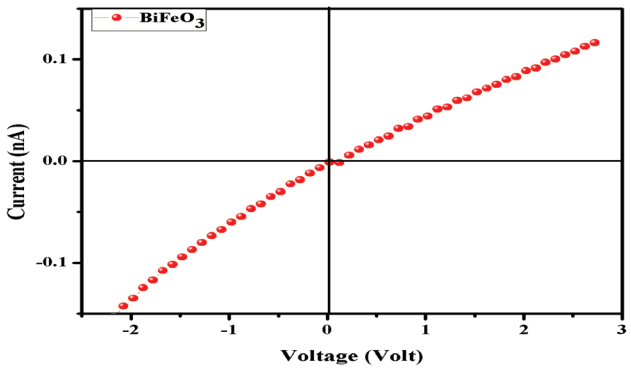

Fig. 4. Current–voltage plot by optimized sample (BFO-(iv)-03).

4.1. Photocatalytic degradation experiment

The experiment was performed in aqueous solution with initial concentration of 0.5 ppm of dye and 200 mg of nanoparticles of BFO for 100 cm^3 of aqueous colloidal solution. The experiment was conducted in particular assembly that consists of a dark box made up of hard board with an aluminum frame structure. The dark box has dimensions of $2 \times 2 \times 2.5$ ft^3 fitted with suitable light sources (UV/Visible) along with one magnetic stirrer, temperature monitoring thermometer (100°C), small exhaust fan and power supply switches. In first instance, the adsorption–desorption equilibrium was established in the dark and then the photocatalytic experiment was started. A 100 cm^3 solution of Congo Red dye with 0.5 ppm concentration was taken in a transparent glass beaker and put on stirrer in the dark box. After recording the dark adsorption data, the saturated BFO nanoparticles were illuminated with visible light source (tungsten bulb, 200 W). The concentration of dye was monitored by spectrophotometer with time interval of 3 min up to 42 min as shown in Fig. 6(c). The photocatalytic efficiency of BFO nanoparticles was measured by plotting the graph between time interval vs. A/A_o as shown in Fig. 6(d).

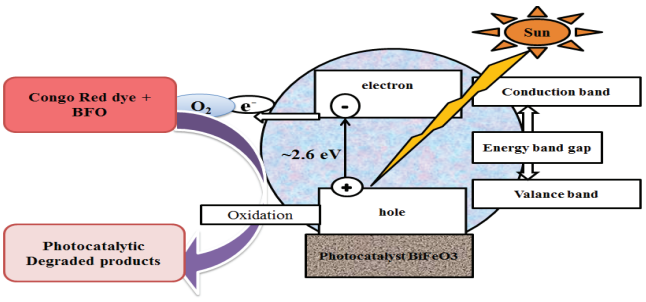

Fig. 5. Schematic diagram of photocatalytic mechanism.

4.2. Characterization of photocatalytic degraded sample

The photodegraded reaction mixture was centrifuged at 10,000 rpm (Scilogex, USA) for 5 min. The sample was characterized through chromatographic analysis and chemical oxygen demand (COD) measurements. A fraction of sample (1 cm^3) was prepared for high-performance liquid chromatography (HPLC) analysis. After filtering sample with 0.45 micron disposable filter (13 mm diameter), 10 μL sample was injected to HPLC (Sykam, Germany) with operating conditions; C-18 column, grain size 0.45 μm, flow rate 1 mL/min, mobile phase; 0.34 % H_3PO_4 (pH < 3): acetonitrile (77:23) and UV/Visible detector (diode-array detector) with wavelength scan from 200 to 800 nm. The chromatogram is shown in Fig. 7.

COD measurements were made by following the reported procedure [27] by using Merck reagents (COD vials), COD incubator and COD meter. 2 cm^3 of each sample (treated and untreated) was added in low range COD vials (150 ppm). Similarly for blank and standard, 2 cm^3 of each deionized water and potassium acid pthalate solution 2 cm^3 = 100 mg COD were added in separate COD vials. All four COD vials were incubated up to 2 h at 120°C. After completion of incubation time, COD was estimated through COD-meter. The comparison of COD values for treated and untreated samples are shown in Table 2. The photocatalytic degradation efficiency of BFO in terms of COD was calculated by applying the following formula:

$$\text{Chemical oxygen demand Removal (\%)} = \frac{[\text{COD for untreated} - \text{COD for treated}]}{\text{COD for untreated}} \times 100$$

The COD value for treated sample was calculated to be 63.56% less than the untreated sample which showed a photodegradation of Congo Red dye into simple hydrocarbon products as observed in HPLC-chromatogram.

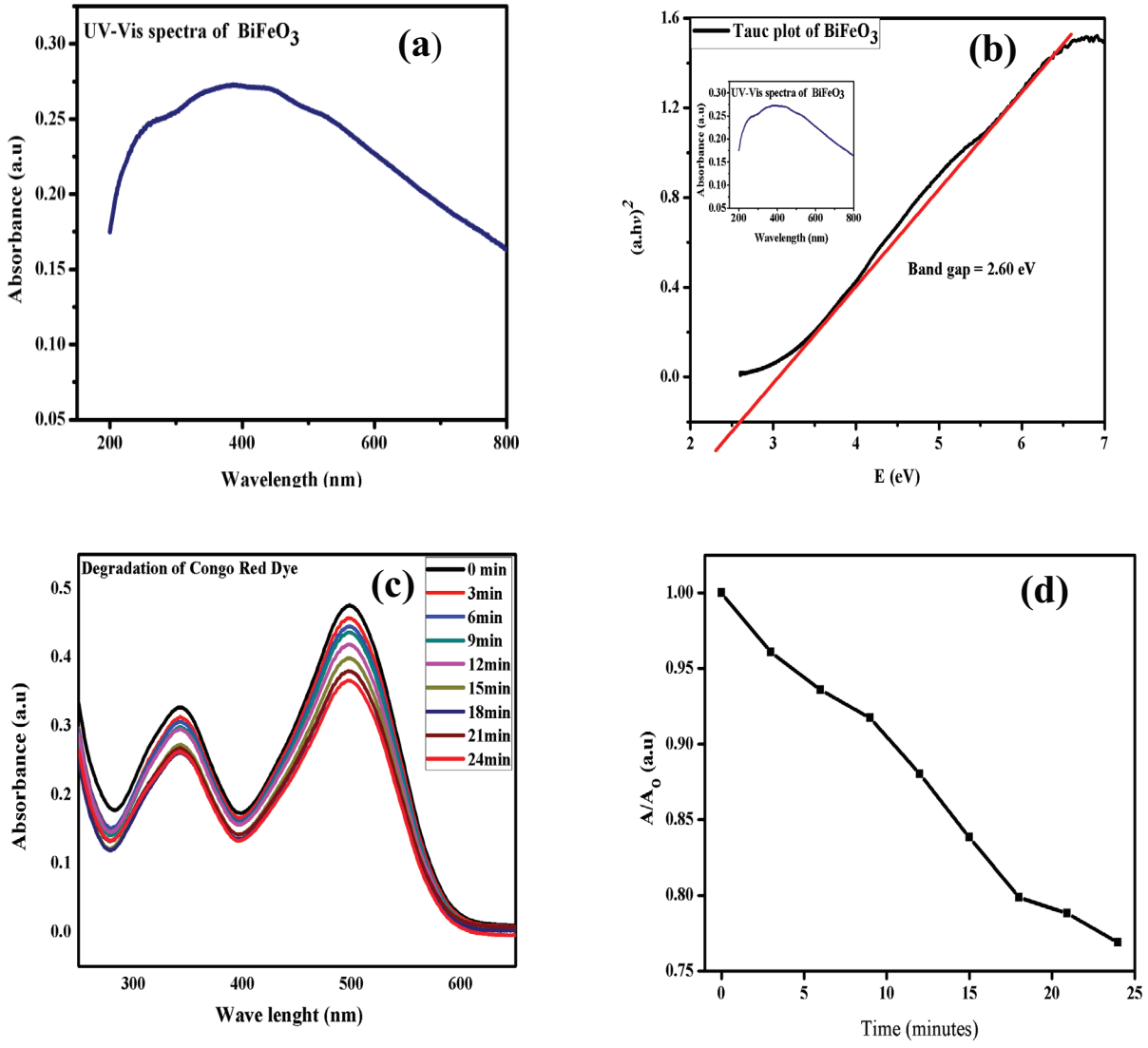

Fig. 6. (a) UV/Visible spectrum of optimized sample, (b) Tauc plot of optimized sample, (c) photocatalytic degradation of Congo Red. (d) A plot between A/A_o vs. time (minutes) photocatalytic degradation of Congo Red.

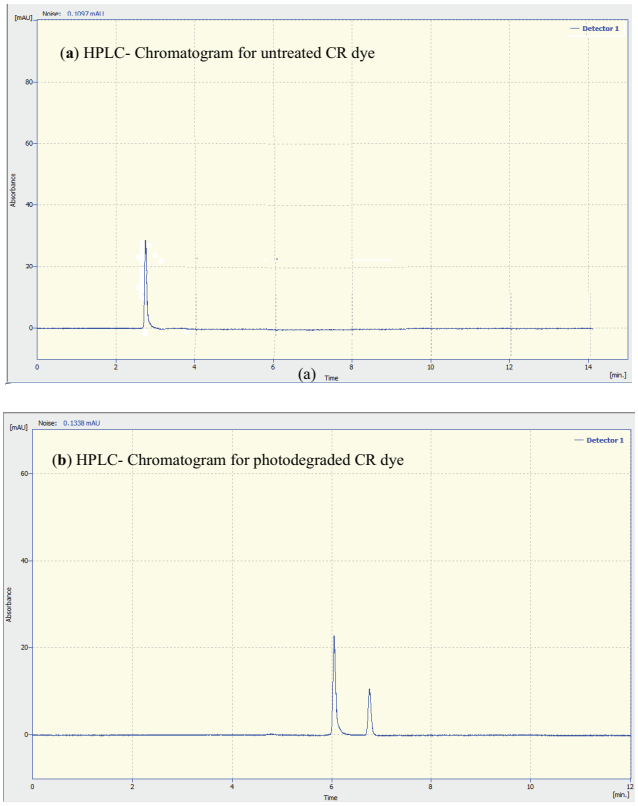

Fig. 7. HPLC-chromatogram of untreated (a) and photocatalytic degraded Congo Red dye (b).

Table 2
COD estimation for untreated and treated samples of Congo Red dye

Reagent blank COD (mg)	0.002
Standard COD estimation (mg)	
Assigned value	100
Measured value	98.78
COD estimation for untreated sample (mg)	102.31
COD estimation for treated sample (mg)	37.47
COD differences (mg)	64.84
COD removal (%)	63.56

5. Stability of BFO material

The BFO nanoparticles were investigated for post structural stability by comparing the XRD pattern after application in photocatalytic degradation experiment. The XRD pattern was exactly same as obtained before application for photocatalytic degradation (Fig. 8). It could be extracted from results that BFO nanoparticles are resistant to any physical and chemical damages during the experiment.

6. Conclusion

BFO has been synthesized with new and low-cost single surfactant micro-emulsion technique. The optimization of various reaction parameters was monitored. It was observed

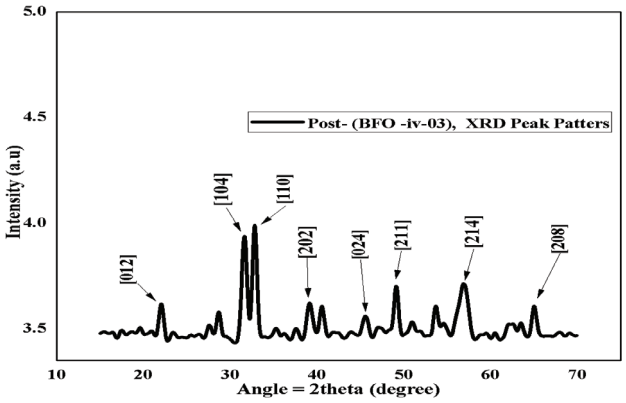

Fig. 8. Post-XRD spectrum for BFO-iv-03 (after photocatalytic degradation application for Congo Red dye).

that the addition of co-surfactant increased the flexibility of micro-emulsion reaction mixture. $Bi(NO_3)_3.5H_2O$ and $BiCl_3$ were soluble in concentrated HNO_3 and the acid strength may be diluted up to pH value ~1.5. The use of $BiCl_3$ instead of $Bi(NO_3)_3.5H_2O$ evoked pronounced results. The annealing temperature was estimated by TGA/DSC curves which exhibited insignificant weight loss beyond 820°C. All the samples were annealed at same range of temperatures, that is, 800°C, 850°C and 900°C in the same furnace. The optimized results were obtained for the sample (BFO-(iv)-03). This sample was annealed at 900°C for 7 h. The crystallite size was found to be <20 nm, which is useful for many advanced technological applications. The optimized sample was also subjected for UV/Visible scan and optical band gap was measured by Tauc plot in the range of ~2.6 eV. The conductivity was measured by current–voltage relation in the range of 1.005×10^{-9} S cm^{-1}. The fabricated BFO was investigated for photocatalytic activity. The photodegradation analysis of Cong Red dye was carried out and very good results were obtained. The treated sample was investigated through HPLC and COD values for treated and untreated samples. Both the techniques exposed a photodegradation of Congo Red dye into simple hydrocarbon products. The post XRD characterization showed chemical and physical stability during the photoreaction and suggested the recyclability of the prepared photocatalyst material.

Acknowledgments

Authors (I. Shakir, M. Sarfraz and M.F.A. Aboud) are thankful to the King Saud University, Riyadh, Saudi Arabia, for funding through research grant no. RGP-VPP-312. Other authors are grateful to the Islamia University of Bahawalpur and Higher Education Commission of Pakistan.

Symbols

BFO	—	$BiFeO_3$
CR dye	—	Congo Red dye
COD	—	Chemical oxygen demand
CTAB	—	Cetyltrimethylammonium bromide
HPLC	—	High-performance chromatography
I-V	—	Current–voltage relation
h	—	Plank's constant

TGA/DSC	—	Thermogravimetric analysis/differential scanning calorimetric
ρ	—	Resistivity
σ	—	Conductivity
υ	—	Photon frequency
XRD	—	X-ray diffraction

References

[1] W. Eerenstein, N.D. Mathur, J.F. Scott, Multiferroic and magnetoelectric materials, Nature, 442 (2006) 759–765.

[2] P. Kharel, C. Sudakar, A. Dixit, A.B. Harris, R. Naik, G. Lawes, Electric-field control of a magnetic phase transition in $Ni_3V_2O_8$, Europhys. Lett., 86 (2009) 17007.

[3] Y.-H. Chu, L.W. Martin, M.B. Holcomb, R. Ramesh, Controlling magnetism with multiferroics, Mater. Today, 10 (2007) 16–23.

[4] J. Silva, A. Reyes, H. Esparza, H. Camacho, L. Fuentes, $BiFeO_3$: a review on synthesis, doping and crystal structure, Integr. Ferroelectr., 126 (2011) 47–59.

[5] E. Mostafavi, A. Ataie, M. Ahmadzadeh, Characterization of nano-structured multiferroic bismuth ferrite produced via solid state reaction route, Adv. Mater. Res., 829 (2014) 683–687.

[6] R. Safi, H. Shokrollahi, Physics, chemistry and synthesis methods of nanostructured bismuth ferrite ($BiFeO_3$) as a ferroelectro-magnetic material, Prog. Solid State Chem., 40 (2012) 6–15.

[7] G. Ali, S. Siddiqi, S. Ramay, S. Atiq, M. Saleem, Effect of co substitution on the structural, electrical, and magnetic properties of $Bi_{0.9}La_{0.1}FeO_3$ by sol-gel synthesis, Int. J. Miner. Metall. Mater., 20 (2013) 166–171.

[8] L.L. Hench, J.K. West, The sol-gel process, Chem. Rev., 90 (1990) 33–72.

[9] J.H. Schulman, W. Stoeckenius, L.M. Prince, Mechanism of formation and structure of micro emulsions by electron microscopy, J. Phys. Chem., 63 (1959) 1677–1680.

[10] C. Tojo, M. Blanco, M. López-Quintela, Microemulsions as microreactors: a Monte Carlo simulation on the synthesis of particles, J. Non-Cryst. Solids, 235 (1998) 688–691.

[11] C. Solans, P. Izquierdo, J. Nolla, N. Azemar, M. Garcia-Celma, Nano-emulsions, Curr. Opin. Colloid Interface Sci., 10 (2005) 102–110.

[12] G. Palazzo, F. Lopez, M. Giustini, G. Colafemmina, A. Ceglie, Role of the Cosurfactant in the CTAB/water/n-pentanol/n-hexane water-in-oil microemulsion. 1. Pentanol effect on the microstructure, J. Phys. Chem. B, 107 (2003) 1924–1931.

[13] P. Ayyub, A. Maitra, D.O. Shah, Microstructure of the CTAB-butanol-octane-water microemulsion system: effect of dissolved salts, J. Chem. Soc. Faraday Trans., 89 (1993) 3585–3589.

[14] M.A. Malik, M.Y. Wani, M.A. Hashim, Microemulsion method: a novel route to synthesize organic and inorganic nanomaterials: 1st nano update, Arab. J. Chem., 5 (2012) 397–417.

[15] M. Boutonnet, S. Lögdberg, E.E. Svensson, Recent developments in the application of nanoparticles prepared from w/o microemulsions in heterogeneous catalysis, Curr. Opin. Colloid Interface Sci., 13 (2008) 270–286.

[16] F. Chen, G.-Q. Xu, T.S.A. Hor, Preparation and assembly of colloidal gold nanoparticles in CTAB-stabilized reverse microemulsion, Mater. Lett., 57 (2003) 3282–3286.

[17] N. Vlachopoulos, P. Liska, J. Augustynski, M. Grätzel, Very efficient visible light energy harvesting and conversion by spectral sensitization of high surface area polycrystalline titanium dioxide films, J. Am. Chem. Soc., 110 (1988) 1216–1220.

[18] A. Fujishima, Electrochemical photolysis of water at a semiconductor electrode, Nature, 238 (1972) 37–38.

[19] J. Wang, J. Neaton, H. Zheng, V. Nagarajan, S. Ogale, B. Liu, D. Viehland, V. Vaithyanathan, D. Schlom, U. Waghmare, Epitaxial $BiFeO_3$ multiferroic thin film heterostructures, Science, 299 (2003) 1719–1722.

[20] S. Zhang, J. Li, M. Zeng, G. Zhao, J. Xu, W. Hu, X. Wang, In situ synthesis of water-soluble magnetic graphitic carbon nitride photocatalyst and its synergistic catalytic performance, ACS Appl. Mater. Interfaces, 5 (2013) 12735–12743.

[21] H. Wang, W. He, X.A. Dong, G. Jiang, Y. Zhang, Y. Sun, F. Dong, In situ DRIFT investigation on the photocatalytic NO oxidation mechanism with thermally exfoliated porous gC_3N_4 nanosheets, RSC Adv., 7 (2017) 19280–19287.

[22] T.T. Carvalho, P.B. Tavares, Synthesis and thermodynamic stability of multiferroic $BiFeO_3$, Mater. Lett., 62 (2008) 3984–3986.

[23] P. Hermet, M. Goffinet, J. Kreisel, P. Ghosez, Raman and infrared spectra of multiferroic bismuth ferrite from first principles, Phys. Rev. B, 75 (2007) 220102.

[24] S. Greicius, J. Banys, I. Szafraniak, A. Kholkin, Conductivity Investigations of Pure and Ba, Ca, Sr Doped BiFeO, 2009 18th IEEE International Symposium on the Applications of Ferroelectrics, 2009, pp. 1–3.

[25] S. Erdemoğlu, S.K. Aksu, F. Sayılkan, B. İzgi, M. Asiltürk, H. Sayılkan, F. Frimmel, Ş. Güçer, Photocatalytic degradation of Congo Red by hydrothermally synthesized nanocrystalline TiO_2 and identification of degradation products by LC–MS, J. Hazard. Mater., 155 (2008) 469–476.

[26] B. von Blanckenhagen, D. Tonova, J. Ullmann, Application of the Tauc-Lorentz formulation to the interband absorption of optical coating materials, Appl. Opt., 41 (2002) 3137–3141.

[27] A.M. Jirka, M.J. Carter, Micro semiautomated analysis of surface and wastewaters for chemical oxygen demand, Anal. Chem., 47 (1975) 1397–1402.